NASA/TM–2019–220281

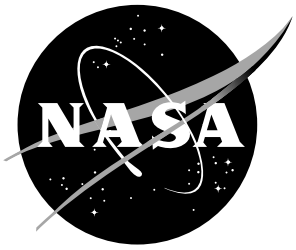

In-Space Robotic Assembly Joint Characterization Approach

Nijo A. Abraham, Richard K. Bird, and William R. Doggett
Langley Research Center, Hampton, Virginia

Timothy S. Roach
Science and Technology Corporation, Hampton, Virginia

May 2019

NASA STI Program. . . in Profile

Since its founding, NASA has been dedicated to the advancement of aeronautics and space science. The NASA scientific and technical information (STI) program plays a key part in helping NASA maintain this important role.

The NASA STI Program operates under the auspices of the Agency Chief Information Officer. It collects, organizes, provides for archiving, and disseminates NASA's STI. The NASA STI Program provides access to the NASA Aeronautics and Space Database and its public interface, the NASA Technical Report Server, thus providing one of the largest collection of aeronautical and space science STI in the world. Results are published in both non-NASA channels and by NASA in the NASA STI Report Series, which includes the following report types:

- TECHNICAL PUBLICATION. Reports of completed research or a major significant phase of research that present the results of NASA programs and include extensive data or theoretical analysis. Includes compilations of significant scientific and technical data and information deemed to be of continuing reference value. NASA counterpart of peer-reviewed formal professional papers, but having less stringent limitations on manuscript length and extent of graphic presentations.

- TECHNICAL MEMORANDUM. Scientific and technical findings that are preliminary or of specialized interest, e.g., quick release reports, working papers, and bibliographies that contain minimal annotation. Does not contain extensive analysis.

- CONTRACTOR REPORT. Scientific and technical findings by NASA-sponsored contractors and grantees.

- CONFERENCE PUBLICATION. Collected papers from scientific and technical conferences, symposia, seminars, or other meetings sponsored or co-sponsored by NASA.

- SPECIAL PUBLICATION. Scientific, technical, or historical information from NASA programs, projects, and missions, often concerned with subjects having substantial public interest.

- TECHNICAL TRANSLATION. English-language translations of foreign scientific and technical material pertinent to NASA's mission.

Specialized services also include organizing and publishing research results, distributing specialized research announcements and feeds, providing information desk and personal search support, and enabling data exchange services.

For more information about the NASA STI Program, see the following:

- Access the NASA STI program home page at `http://www.sti.nasa.gov`

- E-mail your question to `help@sti.nasa.gov`

- Phone the NASA STI Information Desk at 757-864-9658

- Write to:
  NASA STI Information Desk
  Mail Stop 148
  NASA Langley Research Center
  Hampton, VA 23681-2199

NASA/TM–2019–220281

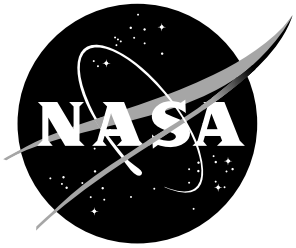

In-Space Robotic Assembly Joint Characterization Approach

Nijo A. Abraham, Richard K. Bird, and William R. Doggett
Langley Research Center, Hampton, Virginia

Timothy S. Roach
Science and Technology Corporation, Hampton, Virginia

National Aeronautics and
Space Administration

Langley Research Center
Hampton, Virginia 23681-2199

May 2019

Available from:

NASA STI Program / Mail Stop 148
NASA Langley Research Center
Hampton, VA 23681-2199
Fax: 757-864-6500

TABLE OF CONTENTS

LIST OF FIGURES

LIST OF ACRONYMS

BAA	Broad Agency Announcement
CNC	Computer Numerical Control
EVA	Extravehicular Activity
GEO	Geostationary Earth Orbit
HIP	Hot Isostatic Pressing
HVAC	Heating, Ventilation and Air Conditioning
ISA	In-Space Assembly
LaRC	Langley Research Center
LVDT	Linear Variable Displacement Transducer
NASA	National Aeronautics and Space Administration
SMR	Spherically Mounted Retroreflector
TDM	Technology Demonstration Mission

LIST OF SYMBOLS

E	Young's modulus of elasticity
G	Shear modulus of elasticity
I	Bending moment of inertia
J	Torsional constant
P	Load applied
A	Area of cross-section
L	Length of test specimen
δ	Average displacement of LVDTs during axial test
θ	Rotation of bending curve at origin
y	Displacement of the specimen along the bending curve
φ	Torsional angular twist of specimen
T	Torque applied

IN-SPACE ROBOTIC ASSEMBLY JOINT CHARACTERIZATION APPROACH

ABSTRACT

This paper describes the test systems and approaches developed to characterize the performance of a structural joint that is intended for robotic in-space assembly (ISA). The design of the joint is based on a heritage concept from National Aeronautics and Space Administration (NASA) Langley Research Center (LaRC) originally intended for structural assembly by astronauts during extravehicular activity (EVA). Its design was modified under a public-private partnership and is intended to accelerate the availability of, and reduce costs for the infusion of NASA developed technologies into commercial ISA systems. Test systems were developed to measure the axial, bending, and torsional stiffness of the joint at a wide range of temperatures. A test system was also developed to measure the reliability of the joint in terms of translation and rotation when disassembled and re-assembled in space. These test systems were used to characterize the joint behavior and provide performance data for the iterative joint design process. The paper also lists the lessons learned to aid testing of next generation robotic in-space assembly joints.

INTRODUCTION

The joint referenced in this paper is developed as part of a public-private initiative funded through the "Tipping Point" broad agency announcement (BAA) by NASA to commercialize emerging in-space capabilities such as manufacturing, assembly of large spacecraft, servicing, and re-purposing of satellites.[1] The initiative is managed as a Technology Demonstration Mission (TDM) under the NASA Space Technology Mission Directorate.

The application proposed for utilizing this joint will mitigate one of the current limitations of Geostationary Earth Orbit (GEO) satellites in which they are deployed only in their as-launched configurations. In-space robotic self-assembly will provide the commercial satellite manufacturer the ability to maximize the utility of the launch vehicle fairing volume to stow capabilities that can be later incorporated on-orbit through a simple assembly step that uses the joint. Multiple applications are envisioned for the use of this joint technology. The assembly and reconfiguration of multiple large antenna reflectors is used in this paper as an example of a possible future mission.

DISCUSSION OF JOINT DESIGN

The heritage joint on which the current design effort is based was designed for assembly by astronauts during EVAs. This heritage joint, shown in the picture on the left in Figure 1 had a 2-inch diameter cylindrical design and was constructed of aerospace-grade aluminum alloys. The structural testing and performance measurement of this joint, performed at NASA LaRC in the late 1970's through early 1990's, validated its application for manually assembling large erectable space structures.[2] As the current focus turned to robotic assembly, the initial concept of operations for repurposing this joint for the robotic ISA application involved converting the astronaut EVA features to robotically-compatible assembly and actuation.[3] Thus, one joint half will be attached to the main spacecraft boom, with the second joint half attached to a stored reflector boom within the cargo compartment. The picture on the right in Figure 1 shows the current design that was

developed over a course of several design iterations. The features that remained constant between the two designs are the presence of two halves and a proprietary spring-loaded latch mechanism to lock them in place. The joint in the middle of Figure 1 was an intermediate design.

Figure 1. Evolution of Robotic In-Space Assembly Joint.

The current design includes a larger square shape with 4-inch long sides at the interface of the joint halves. The ends of the two halves transition to a 4-inch diameter cylinder to enable mounting to a composite boom of similar size. The square shape combined with a slot and pin feature at the interface aid in precise and reliable alignment between the two halves during assembly. Additional features include a grapple fixture to be grasped by the robotic arm, an optical mount to support a fiducial used with a camera on the robotic arm for closed-loop guidance, and a rotational actuator ('Torquer') that allows the robotic arm to operate the latch mechanism. The joint features on the joint and their relative position to the robotic arm are shown in Figure 2.

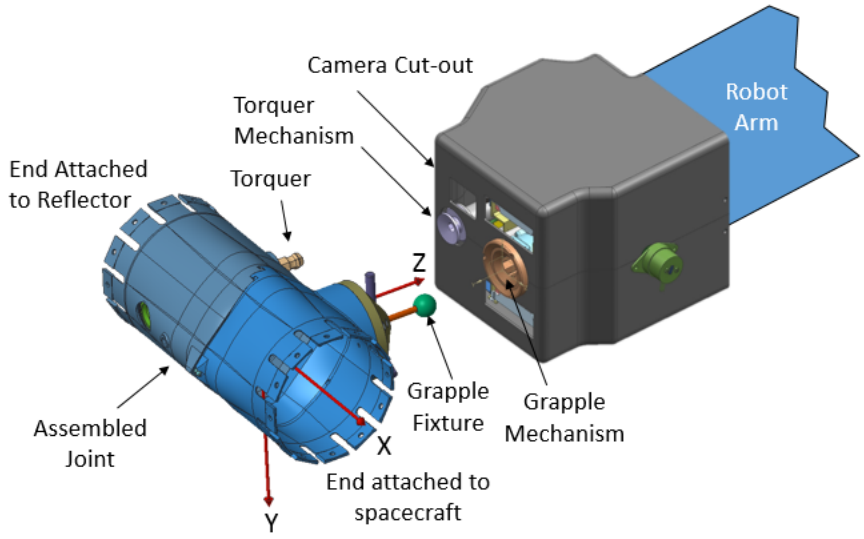

Figure 2. Diagram of the Robotic Arm Engaging the Joint.

The design ensures that the requirements of high stiffness, high strength and low mass needed for these type of ISA structures were not compromised.[4] The joints were fabricated using additive manufacturing of Ti-6Al-4V alloy powder and subjecting the resulting shell to hot isostatic pressing (HIP) for reducing porosity. Contact surfaces between the joint halves and the other features mentioned above were machined using a 5-axis computer numerical control (CNC) machine. The internal latch mechanism and actuation hardware were installed following machining.

Although the square shape helps the four sides come into contact when the latch between the two joint halves is engaged, variation can be introduced at the contact surfaces during fabrication contributing to differences in joint performance during testing. Therefore, after the joint halves were fabricated, a commercially available intensely blue, soft, uniform paste (typically used to identify high spots on bearings) was applied on the contact surfaces of one joint half. Then, after locking and unlocking the two halves, the contact surface of the other joint half was inspected. Figure 3 shows one instance in fabrication variability at the contact surfaces after blue layout aid is applied. The picture on the left shows the ideal contact where all four edges had nearly equal loading (as indicated by blue markings on all edges indicating good contact from the mating part). However, the picture in the center shows an example of a joint that showed poor contact along one of the sides (no blue markings). The quality of the contact at the interface of the joint halves could also be inferred from axial and torsion tests that are mentioned later in this paper. Fabrication was tuned to achieve good contact on all sides.

Figure 3. Variation at Contact Surfaces between Joints shown through Blue Layout Aid.

This paper describes the test systems that were developed and customized to measure the mechanical behavior and the disassembly/re-assembly repeatability for assessing performance improvements associated with iterative joint design. However, due to the proprietary nature of the requirements to which the joint was designed, specific dimensions and performance values will not be mentioned explicitly in this paper.

TEST SYSTEM DEVELOPMENT

There were two sets of tests that were used to characterize joint performance. The first set characterized the structural behavior in terms of stiffness at a proof load based on a factor of safety of 1.5 over the predicted service load. This set had three categories of tests: axial, bending, and torsion that measured the load-displacement or torque-angular displacement behaviors. The second set characterized the mating behavior that included the repeatability of alignment between halves when re-assembled. Each type of test was conducted at -275°F, room temperature, and +320°F to demonstrate that the joints met the strength, stiffness, and re-assembly repeatability requirements over the service temperature range. In addition, the test results were used to provide input to structural models for predicting satellite antenna boom behavior.

A typical joint specimen is shown in Figure 4. The active half is defined as the joint half to which the Torquer was inserted and rotated to unlock and separate the halves along the separation plane. The joint specimen had titanium adapters incorporated into the ends that served as a common interface for the multiple test systems into which it had to be installed.

A key element associated with each of these test types was the necessity of measuring very small displacements over a wide range of temperatures. Digital photogrammetry and laser measurement systems were candidates for small displacement measurements for the mechanical tests, but were not selected due to complexities associated with imaging the specimen within an enclosed environmental chamber and limited visibility associated with the cryogenic test environment. Commercial-off-the-shelf displacement transducers attached directly to the specimen were selected as the method of choice for measuring the small displacements due to their availability, relatively low cost, and adaptability to multiple test environments. A laser tracker system was selected for measuring the small translational and rotational displacements associated with disassembly and re-assembly of the joint specimens.

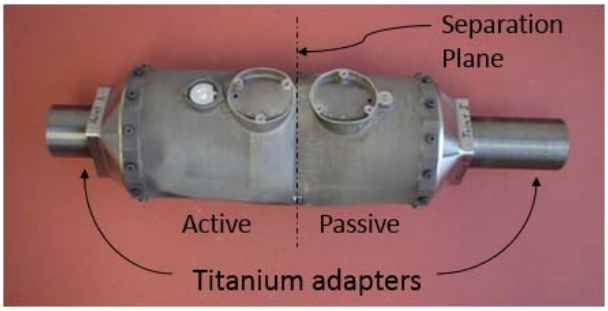

Figure 4. Typical Joint Test Specimen.

LINEAR VARIABLE DISPLACEMENT TRANSDUCER (LVDT) ASSESSMENT AND CALIBRATION

The commercial off-the-shelf LVDTs selected for the mechanical test systems had displacement specifications ranging from ±0.050 inch to ±0.3 inch, depending on the application. They were rated by the manufacturer for an operational temperature range from -40°F to 392°F. Since the cryogenic tests had to be performed at a much lower temperature, tests were conducted on the LVDTs to evaluate their operability at -275°F. Figure 5 shows an LVDT calibration system that was developed with the capability of assessing and calibrating up to six LVDTs simultaneously over the entire temperature range of interest. The LVDTs showed consistent linear displacement-voltage relationship over the displacement range of interest, even at -275°F. Prior to being used for testing, each LVDT was calibrated at each test temperature using a NASA LaRC approved calibration procedure.[5] The extreme temperature calibrations were conducted once the LVDT thermocouples were within 3°F of each other and the average temperature was within ±3°F of the target test temperature. The uncertainty in the LVDT measurements was found to be less than 5% within the displacement range of interest.

Figure 5. LVDT Calibration System.

The ability of the test system to accurately measure specimen displacement and joint stiffness was validated at each test temperature using validation specimens with known dimensions and properties. The pictures of validation specimens for each stiffness measurement test setup are shown later in this paper (Figure 7, Figure 12 and Figure 19). The specimen dimensions were chosen to provide displacements similar to those expected for the joint specimen at the maximum load. Validation specimen stiffnesses were measured experimentally from the slopes of the load-displacement curves of axial and bending tests, and torque-angular displacement of torsion tests. These stiffnesses from experiments were then compared to the respective calculated theoretical stiffnesses. The calibration tests were performed at all three temperatures with tests repeated at least three times at each temperature. The uncertainty associated with each test setup is provided in the subsections below.

AXIAL STIFFNESS TESTS

A test system was developed to conduct axial tension and compression tests on structural joints at -275°F, room temperature, and +320°F to demonstrate that the joints met the strength requirement and to measure the axial stiffness over the service temperature range. The test system utilized a 50,000-lb capacity hydraulic tension-compression test system. The joint specimens were cycled between +300 lbs and -300 lbs at a rate of 200 lbs/minute for four complete cycles. The 300-lb load value represents the combined maximum axial service load in either tension or compression with a factor of safety of 1.5. A diagram of the test system is shown in Figure 6. The top of the specimen was fixed, while load was applied to the bottom end. A 1000-lb in-line load cell was installed at the top of the load train to measure load (P). Rigid LVDT support plates were attached

to the body of each half of the joint with set screws. The specimen displacement was measured using three LVDTs spaced equally around the perimeter of the specimen. The displacement along the centerline (δ) of the specimen was calculated by averaging the three LVDT displacement values. The gage length (L) across which the displacement was measured was nominally 7-8 inches for the joint specimens, depending on the locations on the joint design variants that were amenable to support collar attachment.

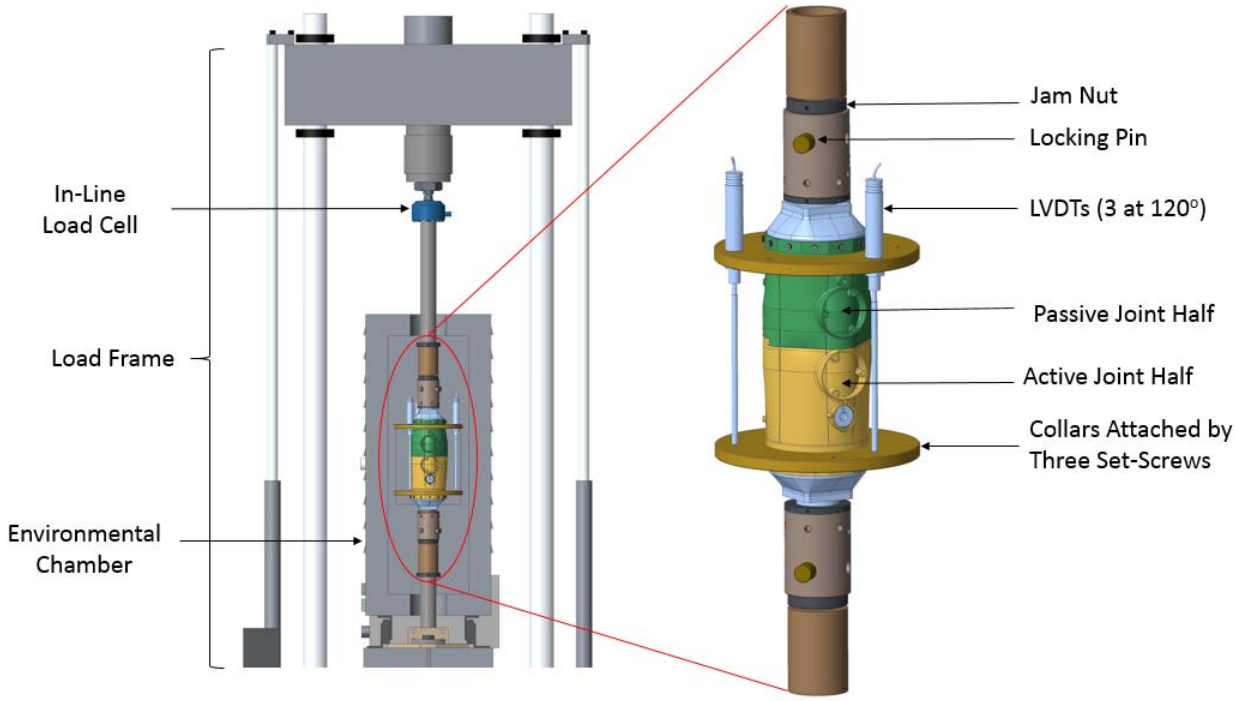

Figure 6. Diagram of Axial Test System.

The axial stiffness (EA/L) was determined from the slope of the load-displacement curve (dP/dδ) generated during the test, as per Equation 1. The stiffness calculations performed at extreme temperatures also took into consideration the effect of temperature on gage length and modulus.

$$EA = \frac{\mathrm{dP}}{\mathrm{d\delta}}.\mathrm{L} \qquad (1)$$

Close-up pictures of the setups for validation and joint specimens are shown in Figure 7. The maximum difference between the experimental and theoretical stiffness values for the validation specimen was 5% over the entire temperature range, indicating that the test system can effectively measure the specimen stiffness behavior, even at these low load and displacement values.

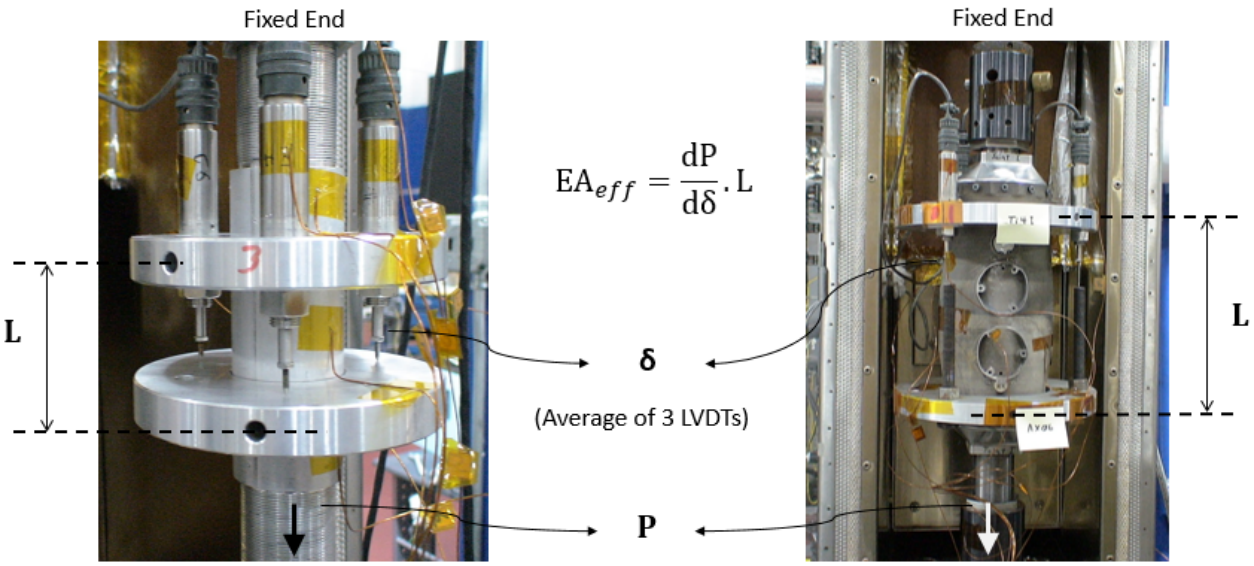

Figure 7. Validation Specimen (Left) and Joint Specimen (Right) Installed in Axial Load Test System.

The typical individual responses of the LVDTs and their average for a joint specimen are shown in Figure 8. The figure highlights the non-linear individual responses that result from the non-uniform loading of the contact areas at low loads or non-axial load through the joint resulting in slight bending during the test. However, the average displacement remained linear. Also, since the joint specimens were tested to only 300 lbs, the maximum average axial displacement was less than 0.0005 inch, which was about 1% of the calibrated range of the LVDTs (±0.01 inch).

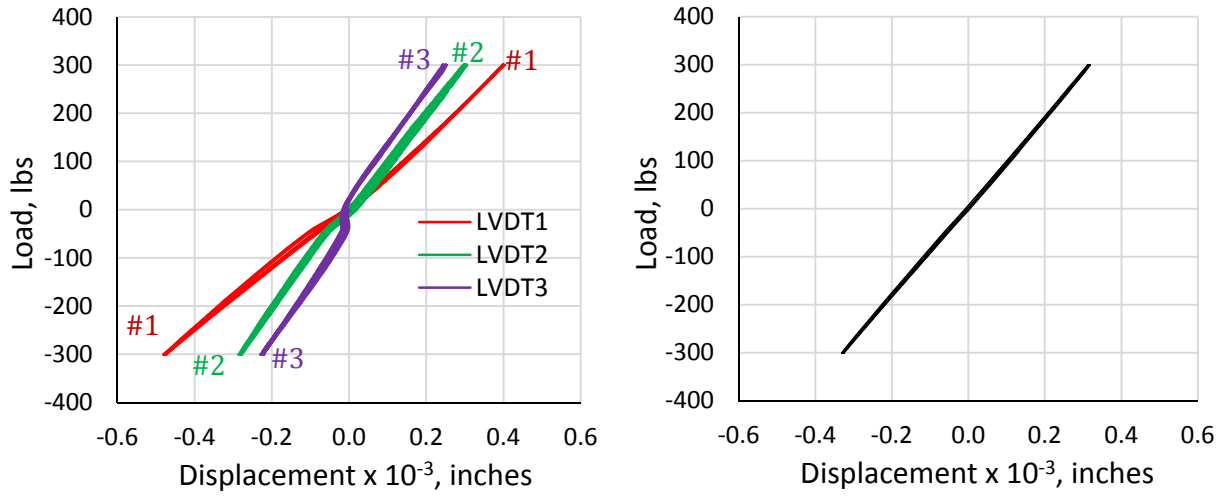

Figure 8. Plots of Load vs. Displacement for Axial Test of a Joint Specimen at Room Temperature: Individual LVDTs (Left) and Average Displacement (Right).

In some of the extreme temperature tests (Figure 9), the average LVDT responses showed shifts in the load-displacement curves of about 0.00005 inch every cycle. This shift was likely due to small lateral shifts in the tips of the LVDTs along the surface of the support plate when the cycles transitioned from loading to unloading. In addition for the cryogenic tests, the cycling of the liquid

nitrogen flow into the chamber to maintain the -275°F test temperature caused small disturbances in the LVDTs and the load-displacement curves. This behavior was observed during the validation specimen and joint specimen tests. Additionally, with respect to joint performance at difference temperatures, Figure 9 shows that for a given load the joint had the least displacement at the cryogenic temperature. The calculated stiffness values matched this observation that the axial stiffness was the highest at the cryogenic temperature.

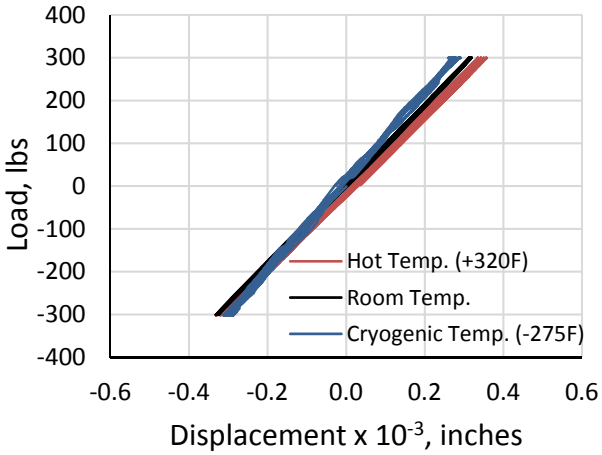

Figure 9. Load vs. Displacement at +320 ºF, Room and -275 ºF for Axial Load Tests.

The axial tests were also indicative of the quality of the contact at the interfaces. Figure 10 shows an example of the load-displacement performance of a joint that had poor contact at the interface as indicated by the blue layout aid during initial mating checks. The non-linear behavior, especially on the compression portion of the curve, indicates poor contact between the surfaces that allowed excessive axial displacement at the small applied loads. For this particular joint, a load much greater than 300 lbs would be needed to establish full contact and generate a linear load-displacement response.

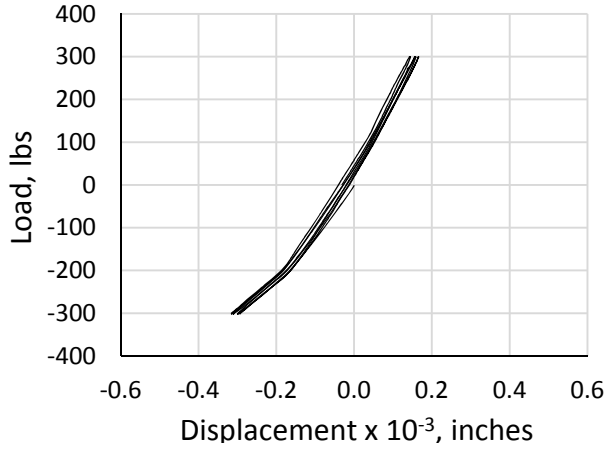

Figure 10. Non-linearity Associated with Poor Contact between Joint Halves.

BENDING STIFFNESS TESTS

A cantilever bend test system was developed to conduct bending tests on the structural joint specimens at -275°F, room temperature, and +320°F to demonstrate that the joints met the bending stiffness, bending moment, and shear strength requirements over the service temperature range. Figure 11 shows a diagram of the test system. A tension-compression load frame was used as a rigid base for the fixed end of the cantilever load column, which consisted of a fixed base bolted to the body of the load frame. The specimen was installed into the test system using load adapters. A titanium riser was installed between the specimen and the base to locate the joint specimen at the desired height relative to the base. Two loading arms were attached to the top of the specimen. Cantilever loads were applied along the positive and negative y-axis directions through the loading arm, using a system of cables, pulleys, and dead weights. The load applied along the cable system was measured using 500-lb capacity in-line load cells. Tables with hydraulically-adjustable height were positioned under the dead weight loads and were used to apply the bending loads in a controlled manner. The joint specimen was cycled between 0 and 150 lbs along the positive y-axis for five cycles, followed by cycling five times over the same load range along the negative y-axis. The 150-lb load value represents the combined maximum shear load seen in orbit with a factor of safety of 1.5 included.

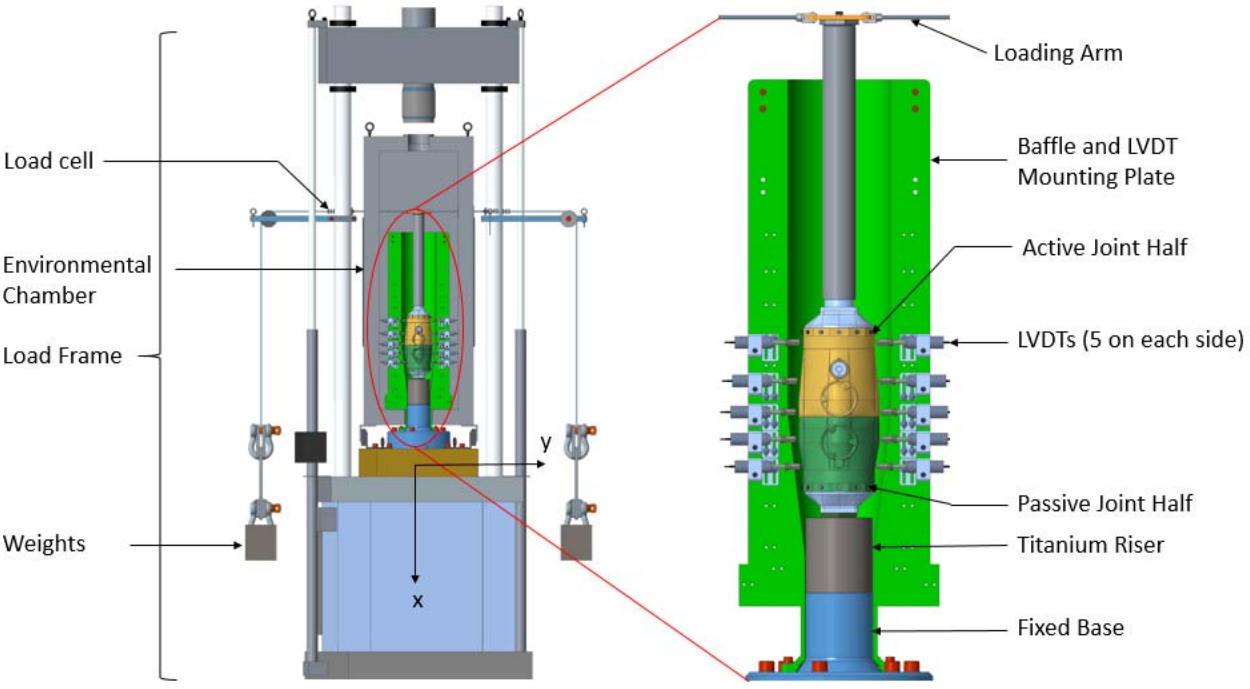

Figure 11. Diagram of Bending Test System.

Lateral displacement parallel to the line of load application (y-axis) was measured at five points along the length of the joint specimen using LVDTs. Figure 11 shows the LVDT configuration in the test system. A rigid LVDT support plate was mounted to the load frame. Brackets were used to attach the LVDT bodies to the support plate such that the LVDT tips contacted the surface of the joint specimen. LVDTs were mounted in diametrically opposing pairs at each measurement location, and the displacement at each location (δ) was calculated by averaging the two opposing

LVDT displacement values. The height location of each LVDT tip was measured relative to the base of the test system using a height gage. The lateral displacement, at the maximum applied load of 150 lbs, was less than 0.01 inch at the bottom-most LVDT location (10% of the rated operating range) and less than 0.03 inch at the top-most LVDT location (30% of the rated operating range).

For tests conducted at elevated and cryogenic temperatures, thermocouples were attached to the surface of the specimen in several locations and to each LVDT. An environmental chamber was used to heat or cool the specimen to the desired test temperature. The chamber was modified with feed-through ports on the sides to allow the cantilever load cables to travel through the walls without interference. The test was conducted once the specimen thermocouples were within 3°F of each other and the average temperature was within ±3°F of the target test temperature.

The average displacement data at 150 lbs for each LVDT pair location was used to derive the bending curve by fitting a cubic polynomial through the data. This bending curve was then used to find the bending stiffness (EI) of the test specimen. The approach taken to find the stiffness from this bending curve took into consideration the rotation about the z axis (θ_0) and displacement along the y axis (y_0) at the origin, by modifying the standard bending curve (Equation 2) to obtain Equation 3. This modification was needed because the boundary condition was not purely fixed for this real world application due to clearance between threads of joint and base. This behavior was in spite of best efforts applying high locking torque and using high tolerance machining. Also, the lower bending moment of inertia at the lower titanium adapter region led to a larger amount of bending below the region of interest that amplified the rotation at the origin. For future applications, it is recommended the adaptor at the bottom has a fixture design that provides a larger bending moment of inertia.

$$y = \frac{P}{6EI}x^2(3l - x) \tag{2}$$

$$y = \frac{P}{6EI}x^2(3l - x) + \theta_0 x + y_0 \tag{3}$$

Figure 12. Bending Test Setup for Idealized Test (Left), Validation Specimen (Center) and Joint Specimen (Right).

$P = applied\ shear\ load$
$l = length\ from\ base\ to\ the\ load\ application\ point$
$a = distance\ from\ base\ to\ the\ first\ measurement\ location$
$x = position\ along\ the\ vertical\ axis$
$y = lateral\ displacement\ taken\ by\ average\ of\ two\ LVDTs\ at\ point\ a$
$y_B = lateral\ displacement\ of\ bending\ column\ at\ point\ B$
$\theta_B = rotation\ of\ bending\ for\ the\ column\ at\ point\ B$
$EI = flexural\ stiffness\ of\ specimen$

Distances l and a, along the heights of the joint and LVDTs from the fixed base, were measured using a calibrated height gauge.

Equation (3) was used to calculate the flexural stiffness using the derivation given in equations (4) through (6). With respect to Figure 12, if the region of interest along the length of the column is section BC, then modifying Equation (3) such that B becomes the point of origin results in

$$y_{BC} = \frac{P}{6EI}x'^2(3l' - x') + \theta_B x' + y_B \quad (4)$$

where, $l' = l - a$; $x' = x - a$;

Therefore, the difference in displacements between the two points B and C gives,

$$y_C - y_B = \frac{P}{6\,EI}\left[{x'_C}^2(3l' - x'_C) - {x'_B}^2(3l' - x'_B)\right] + \theta_B({x_C}' - {x_B}') \quad (5)$$

where, $x'_C = x_c - a$; $x'_B = x_B - a$

Rearranging (5) gives the bending stiffness EI as shown in Equation (6), where θ_B is the coefficient of first-order term of the bending curve.

$$EI = \frac{P}{6}\frac{{x'_C}^2(3l' - x'_C) - {x'_B}^2(3l' - x'_B)}{(y_C - y_B) - \theta_B(x'_C - x'_B)} \quad (6)$$

Similar to the axial test, the ability of the test system to accurately measure the bending behavior of the specimen was validated at each test temperature using a validation specimen as shown in Figure 12. The validation specimen was subjected to the same bending test as the joint specimens. The load-displacement curves at each LVDT location were then used to obtain the bending curve equation at the proof load (Equation 4). This equation was then used to calculate the bending stiffness using Equation 6. The maximum difference between the experimental and theoretical stiffness values was 8% over the range of temperatures tested, indicating that the test system can effectively measure the specimen stiffness behavior.

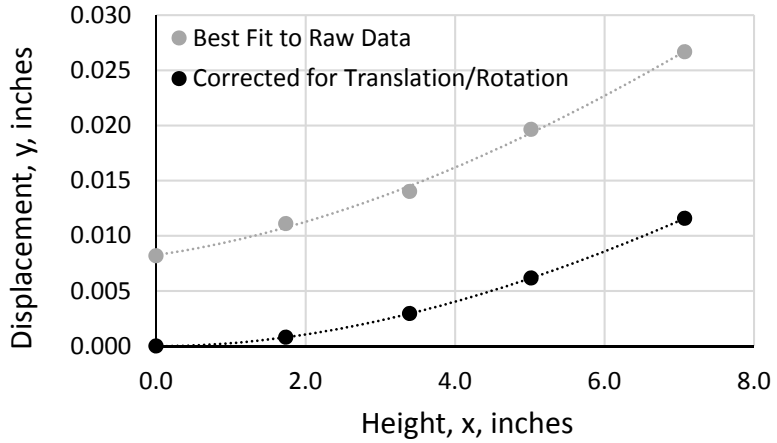

Figure 13. Bending Curve for Joint at 45 Degree Orientation.

A typical bending response for a joint specimen is shown by the lighter curve in Figure 13. The corrected curve is obtained after adjusting for rotation and translation at the origin. The bending stiffness (EI) calculated from the corrected bending curve (for which $\theta_B = 0$ and $y_B = 0$) will lead to the same bending stiffness as applied to the bending curve without corrections.

The load vs. average displacement at each LVDT pair location showed minor hysteresis. Figure 14 shows the typical behavior of the LVDT pair at the highest LVDT pair location. This behavior can be attributed to the test specimen base not being fixed, resulting in a loss of strain energy between loading and unloading.

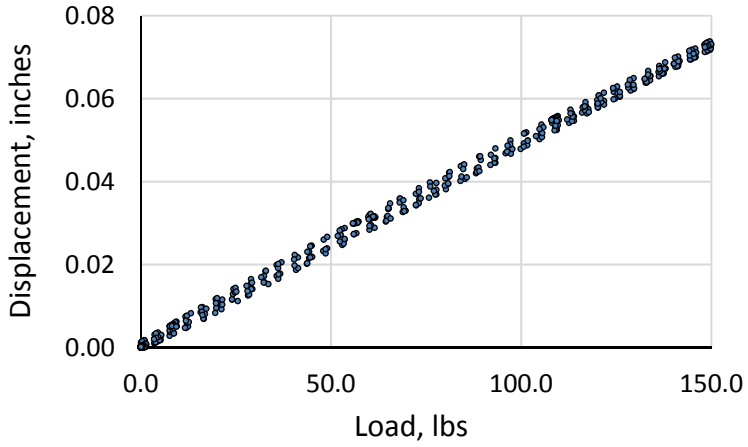

Figure 14. Plot of Load vs. Displacement on an LVDT Pair during Bending Test.

When comparing the bending performance at difference temperatures, the calculated bending stiffness was the highest at the cryogenic temperature. This can be validated by Figure 15 that shows at a given load the joint had the least bending displacement for the cryogenic temperature. Also for extreme temperature tests, the temperature difference along the length of the joint varied approximately 4-5 ^{o}F under cryogenic conditions, and 2-3 ^{o}F for the hot temperature tests. One reason for this non-uniform distribution at each temperature was the high thermal conductivity of the fixed base, which was made of aluminum. The reason for having a larger difference in the

colder condition could be because the liquid nitrogen that was used to cool the test specimen was not sprayed uniformly across the test setup.

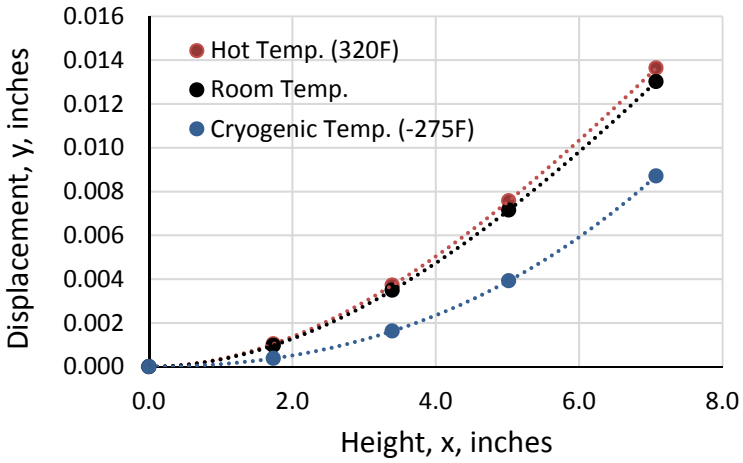

Figure 15. Load vs. Displacement at +320 ºF, Room and -275 ºF for Bending Load Tests.

Since the joint specimen was non-uniform in shape, tests were performed for different orientations with respect to the direction of load application. Figure 16 illustrates the 0º, 45º, 90º and 135º orientations. The 45º and 135º orientations produced the highest amount of pure bending (lowest stiffness) and therefore was used in calculating the baseline bending stiffness of the joint. The 0º and 90º orientations in which the load was applied across the cross-section from corner to corner had the greatest bending stiffness. The least bending stiffness was of interest due to a minimum requirement that the joint had to meet when deployed in orbit.

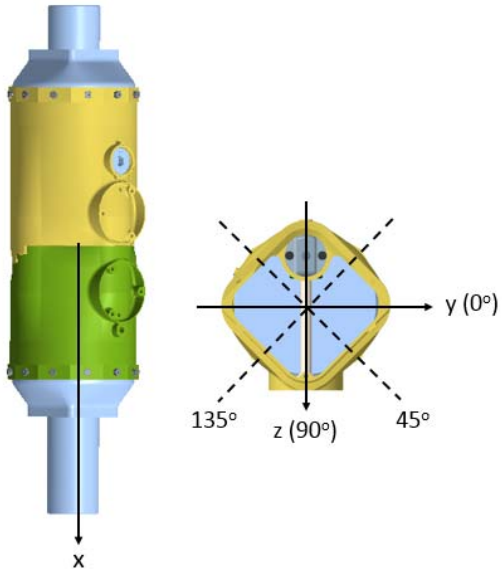

Figure 16. Joint Orientations used for Bending Test.

TORSIONAL STIFFNESS TESTS

A test system was developed to conduct torsion tests on structural joints at -275°F, room temperature, and +320°F to demonstrate that the joints met the strength requirement and to measure the torsional stiffness over the service temperature range. A diagram of the test system is shown in Figure 17. The test system utilized a hydraulic tension-torsion test system with a torque capability of 2500 inch-lbs and axial load capability of ±5000 lbs. The joint specimens were cycled for five complete cycles between +525 inch-lbs and -525 inch-lbs at an angular displacement rate of 3°/minute, as measured by the test machine's angular displacement gage located at the base of the machine (not shown in the diagram). The 525 inch-lbs torque value represents the maximum service torque with a factor of safety of 1.5. The specimen was installed into the load train using coupling adapters. The top of the specimen was attached to the fixed end of the test machine. The axial load was maintained at zero during the torsion cycles by allowing axial displacement. LVDTs were attached using collars to the top and bottom of the specimen with set screws. The collars had diametrically opposing flanges pointing outward from the center of the joint and the flanges were oriented parallel to the support plate. The bodies of four LVDTs were attached to the support plate with the tips of the LVDTs contacting the collar flanges on opposite sides at the top and bottom of the joint specimen.

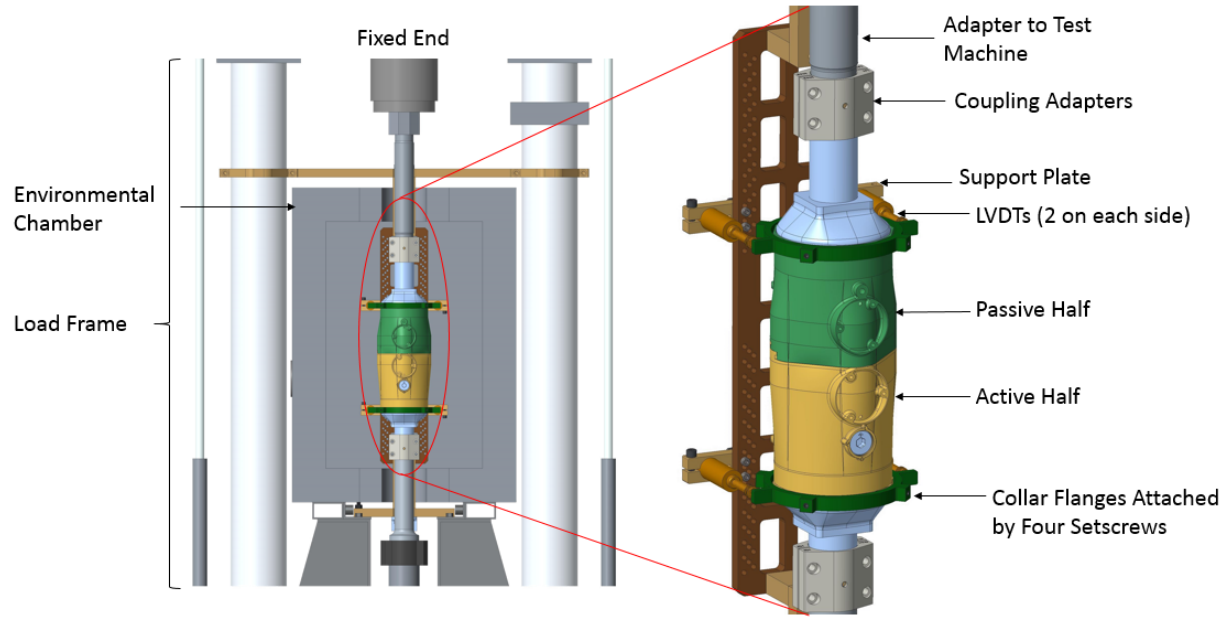

Figure 17. Diagram of Torsion Test System.

The torque applied (T) was measured using an in-line torsion load cell. As the specimen was cycled in torsion, the collar flanges moved along an arc toward and away from the LVDT support plate, thus moving the LVDT cores to measure the linear displacement as shown in Figure 18. Due to the extremely small displacements associated with these tests, the lateral movement of the collar flanges along the arc was ignored and it was assumed that all of the displacement was along the axis of the LVDT. The percent error due to this assumption was approximately 0.3%. The angular displacements at the top and bottom locations were measured by averaging the linear displacement of the two opposing LVDTs (Equation 7) and calculating the rotational angle (φ) associated with that displacement using Equation 8. The specimen angular displacement ($d\varphi$) was calculated as

the difference between the top and bottom angular displacements. The gage length (L) across which the angular displacement was measured was nominally 9 inches when the collars were attached to the faceted ends of the joint specimen. The torsional stiffness (GJ/L) was then determined from the slope of the torque-angular displacement curve (dT/dφ) using Equation 9.

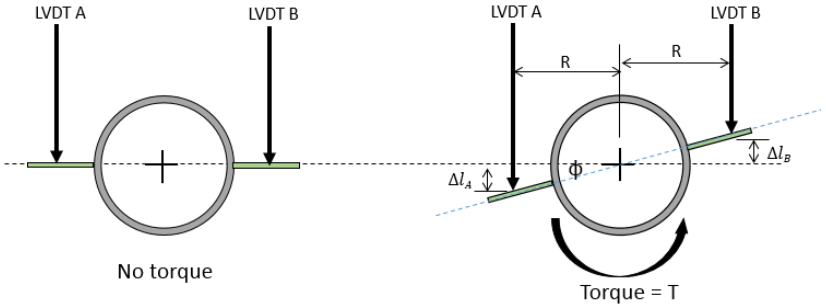

Figure 18. Diagram of Angle of Rotation Calculation.

$$\Delta l = \frac{\Delta l_A + \Delta l_B}{2} \tag{7}$$

$$\varphi \text{ (in radians)} = \tan^{-1}\frac{\Delta l}{R} \tag{8}$$

$$GJ = \frac{\mathrm{dT}}{\mathrm{d}\varphi}.L \tag{9}$$

The close up view of the experimental setups for both the validation specimen and a joint specimen is shown in Figure 19. Since the joint specimens were tested to only 525 inch-lbs, the maximum angular displacements at the top and bottom of the specimen were less than 0.1°. The difference between these angles (specimen angular displacement) was on the order of 0.02°. These angular displacements translated to LVDT linear displacements of less than 0.010 inch (less than 5% of the LVDTs linear range). The ability of the test system to accurately measure specimen angular displacement and joint torsional stiffness was validated at each test temperature using a validation specimen. The validation specimen was subjected to the ±525 in-lbs cyclic torsion test as planned for the joint specimens. Validation specimen stiffness was measured experimentally from the slope of the torque-angular displacement curve and compared to the theoretical stiffness calculated from tube dimensions and properties. The maximum difference between the experimental and theoretical stiffness values was 7% over the complete temperature range, indicating that the test system can effectively measure the specimen stiffness behavior, even at these small displacement values.

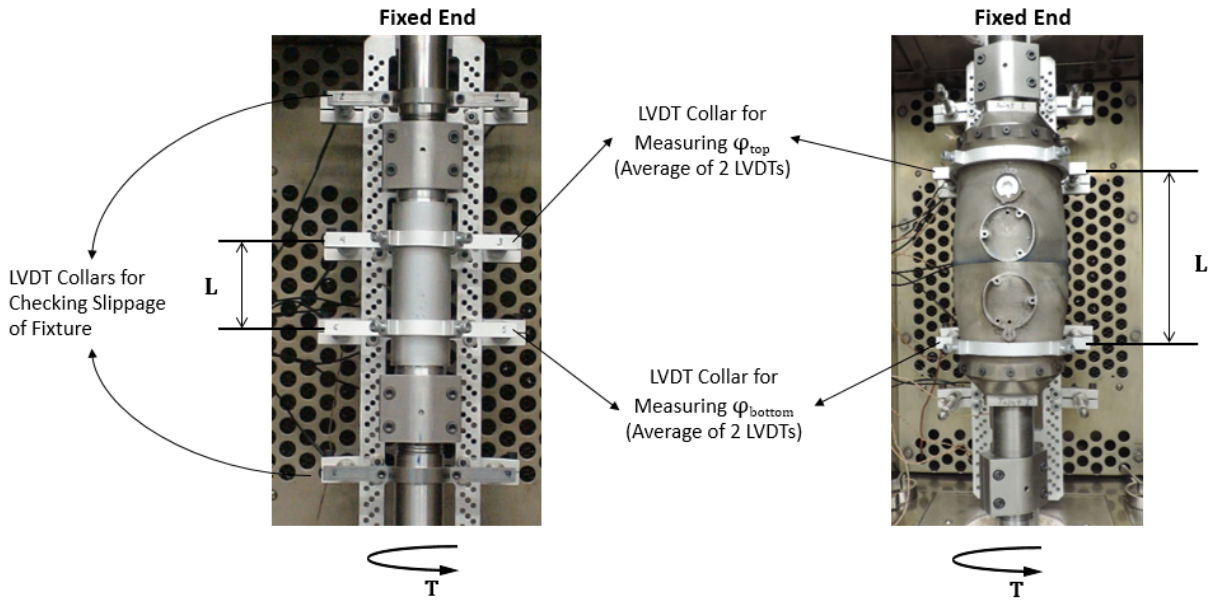

Figure 19. Torsion Test Setup for Validation Specimen (Left) and Joint (Right).

The typical torque vs angular displacement responses seen at the LVDT pairs at the top and bottom of a joint specimen and the derived response are shown in Figure 20. For a maximum load of 550 inch-lbs, the angular displacements at the top and bottom of the specimen were less than 0.15°.

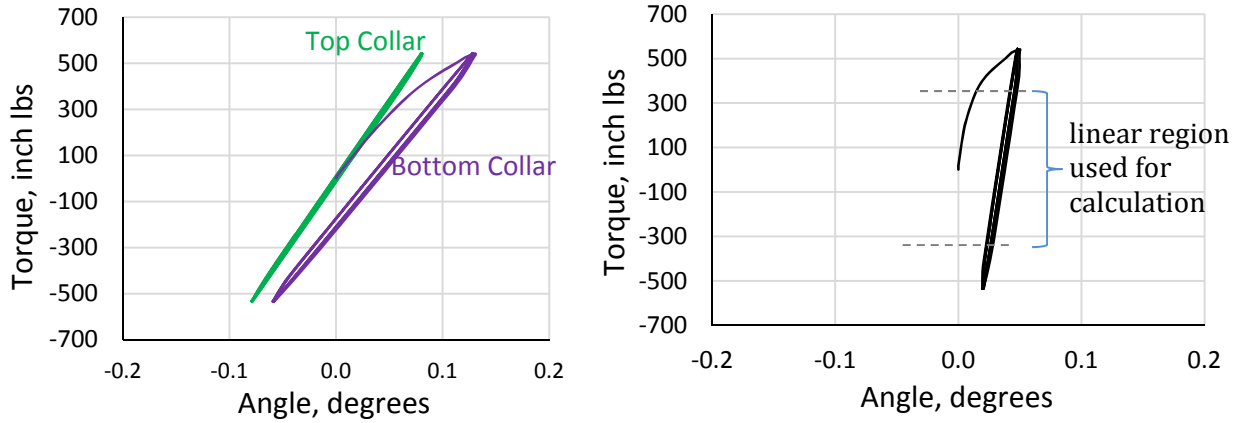

Figure 20. Load vs. Angular Displacement of LVDT-Pairs (left) and Resulting Joint Response (right).

Nonlinearity of the first loading cycle as seen in the right-hand plot of Figure 20 was observed for some of the earlier joints with incomplete contact between the mating surfaces and slight machining roughness affecting the initial seating during the first cycle. Therefore, the first cycle was ignored for the stiffness calculations. Also, varying degrees of hysteresis were observed in these plots for all tests. The individual LVDT responses (left-hand plot of Figure 20) showed that the hysteresis was most prevalent in the torque-displacement curves measured at the bottom half of the joint to which the torque was applied. These LVDTs captured the twist in the joint as well as any rotational translation along the joint mating surfaces once the torque overcame the frictional resistance. This was observed as non-linear behavior at the higher torque values. To avoid this non-linear portion of the torque-displacement curve for the stiffness calculation, only the loading

and unloading cycles within the linear response region between -300 in-lbs and +300 in-lbs were included. This region corresponded to the torque requirement with a factor of safety of 1.5.

Similar to bending and axial load tests, when comparing tests at different temperatures, the cryogenic case had the highest calculated torsional stiffness for the joint. Although crudely, this can be seen from the empirical data shown in Figure 21, where the displacement at a given load was the least for the cryogenic temperature.

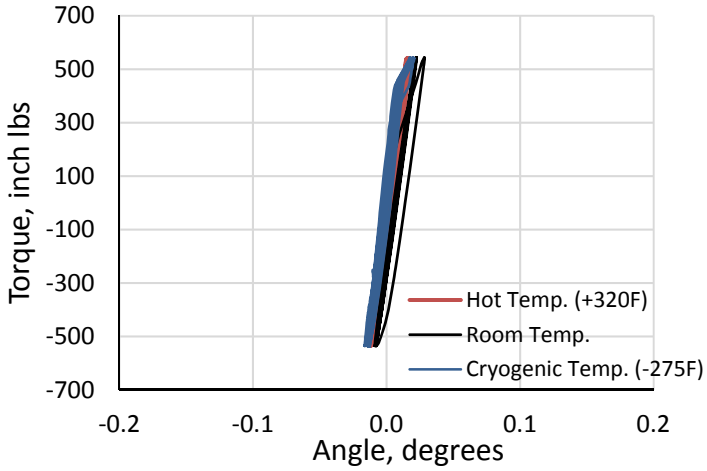

Figure 21. Load vs. Displacement at +320 ºF, Room and -275 ºF for Torsion Load Tests.

Preliminary evaluation of the torsion test system included varying the locations where the LVDT collar set screws were attached to the body of the joint. The set screws were located on the circular cross section region of the thin-walled body with a gage length of nominally 7 inches. The collars were rotated around the circumference of the body and test results were compared to determine if collar locations affected results. These tests resulted in differences in the calculated stiffness of up to 22% when collars were rotated 60° from each other. Finite element analysis was conducted on the joint design to investigate the discrepancy among the calculated stiffness values. The analysis indicated surface distortions in the non-symmetric body of the joint. Figure 22 shows the finite element results with the surface distortions. These distortions caused out-of-plane motion of the collars and incorrect measurement of the angular twist at the tips of the LVDTs. Therefore, the collars were relocated to the faceted ends of the joint (see Figure 23**)** resulting in a gage length of about 9 inches. These regions had a greater wall thickness and were attached to the rigid titanium load adapters, thus providing a stable surface for the collar attachment points. At the new locations the difference in calculated stiffness values between orientations differing by 60º was reduced to less than 5%.

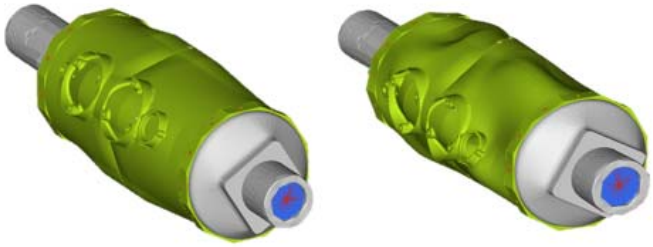

Figure 22. Analysis Results Showing Surface Distortions: before Applying Torque (left) and after Applying Torque (right).

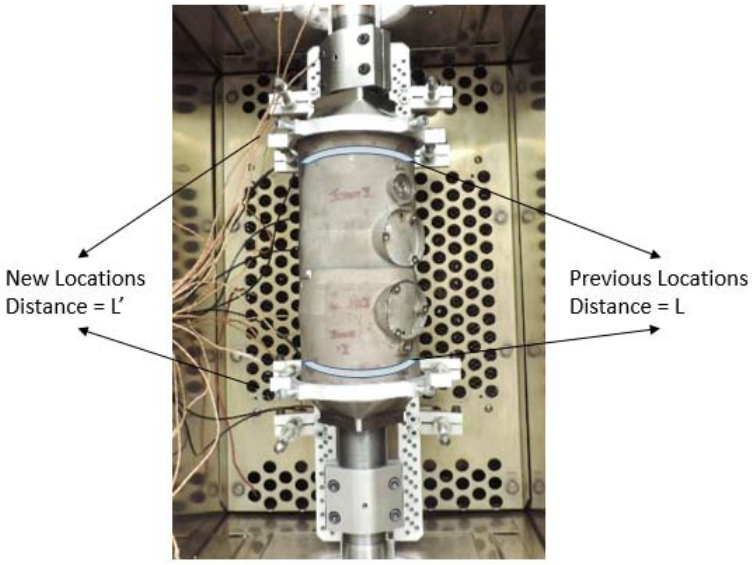

Figure 23. Two Versions of Collar Locations for Torsion Test.

For later design iterations of the joint, alignment features such as cylindrical and square pins were added to each joint half to ensure the two halves engaged each other at the same position after re-assembly (see Figure 24). Prior to machining these features, a torsion test was conducted on the locked joint to pre-seat the two halves. Machining was then performed on the locked joint, without separating the halves. Torsion tests were conducted following pin installation to observe changes to the hysteresis behavior and provide a preliminary assessment on any improvement in joint performance with the alignment features. Figure 23 shows an example of torque-angular displacement curves from a pre-seat torsion test and a test following pin installation. Repeatable re-assembly was associated with lower hysteresis and reduced non-linear response for the first loading cycle.

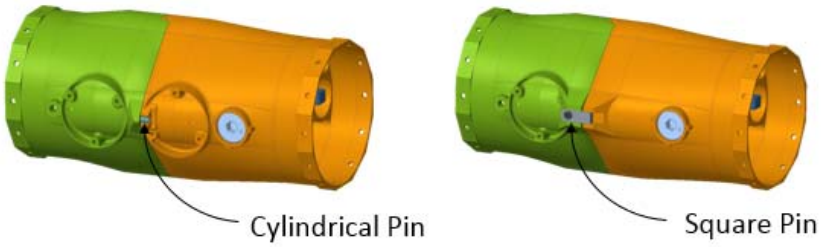

Figure 24. Alignment Features between using Cylindrical (Left) and Square (Right) Pins.

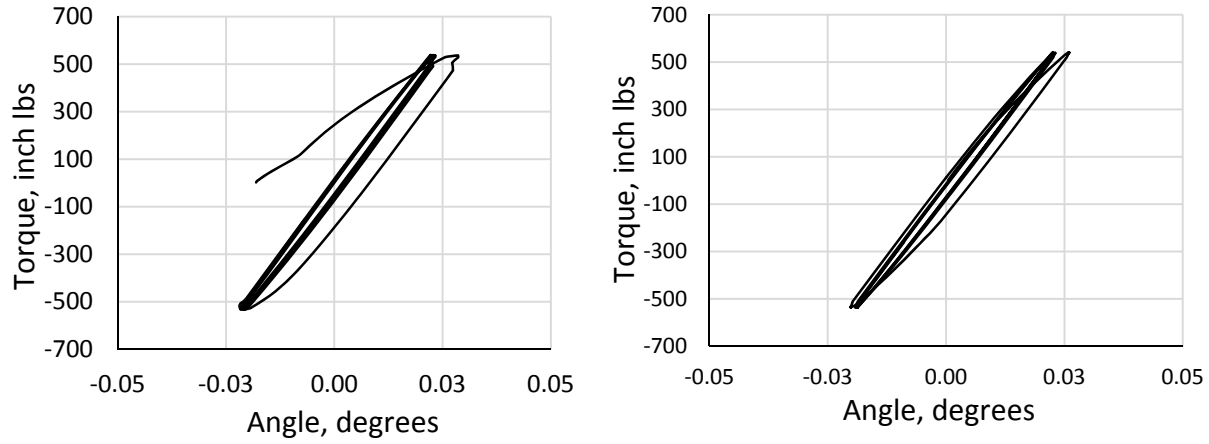

Figure 25. Joint Torsion Test Performance Before (Left) and After (Right) Installation of the Square Pin Alignment Feature.

REPEATABILITY MEASUREMENT TESTS

The repeatability test was used to measure the change in position of the joint halves relative to each other (translational and rotational) after re-assembly. Figure 26 shows a joint specimen installed for the repeatability test, with the active half attached to the joint mounting fixture. Selected positions on each joint half were measured using two laser tracker coordinate measuring machines with interferometer technology. The coordinates of the joint halves were marked using spherically mounted retroreflectors (SMRs) placed on two nests that had been adhesively bonded to the joint halves. The two laser trackers were then used, each marking the location of an SMR. Both trackers used a common coordinate system. The coordinate system of the joint, shown in Figure 27, was defined with the x-axis along the centerline of the joint. The z-axis was parallel to the centerline of the Torquer mechanism.

Since the repeatability measurements required extreme precision on the order of less than 100 microinches, several steps were taken to increase test system stability. Errors caused by using both the horizontal and vertical angle encoders of the laser measurement system were minimized by placing the nests at the same height. The environmental effects were minimized by ensuring heating, ventilation, and air conditioning (HVAC) systems in the vicinity of the tracker were turned off. The test table was placed on rubber pads to dampen ground vibrations. The laser tracker was turned on and allowed to stabilize for at least 6 hours before measurements were taken to minimize changes that occur during warming of the device. Furthermore, the data acquisition parameters were defined to improve accuracy by calculating each data point from an average of samples taken over an interval of 5 seconds. Also, measurements were set to be taken only when the stability of captured data was within 0.0002 inch. These parameters, including the locations of the laser trackers, were determined using a trial and error method.

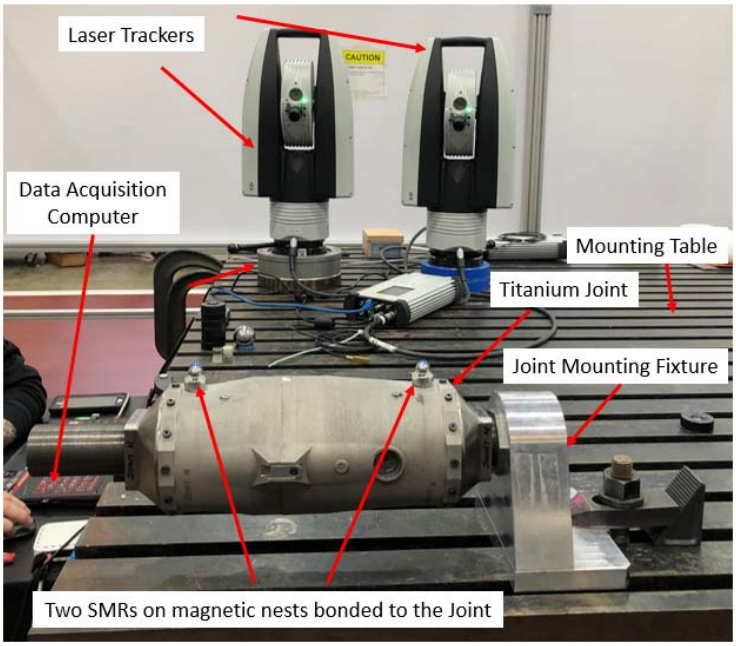

Figure 26. Test System used for Repeatability Measurement.

An initial set of 10 measurements was taken without disassembling the joint to determine the precision of the test system. The joint assembly repeatability measurements involved disassembling and assembling the joint 10 times followed by taking coordinate measurements for each assembled configuration. The angular rotation between the two halves along the x-axis of Figure 27 was calculated using the dot product of their vector projections onto the normal plane. The rotation about the x-axis was calculated per Equation 10. The repeatability of the joint assembly about each axis was then determined from the standard deviations of these rotations and translations. A statistical confidence of 95% was used (2 standard deviations) to design the joint whose two halves consistently assembled with a deviation of less than 0.01 inch and 0.01°. This test setup was able to achieve a precision of 0.00008 inches and 0.0008 °.

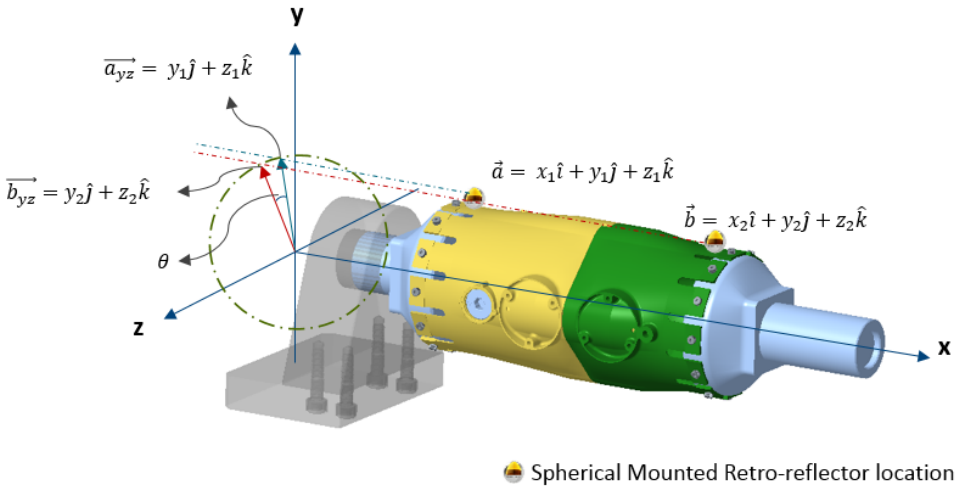

Figure 27. Joint Coordinate System and Vector Calculation for Repeatability Measurement.

$$\cos\theta = \frac{\overrightarrow{a_{yz}} \cdot \overrightarrow{b_{yz}}}{|\overrightarrow{a_{yz}}||\overrightarrow{b_{yz}}|} = \frac{y_1\, y_2 + z_1\, z_2}{\sqrt{y_1^2+z_1^2}\,\sqrt{y_2^2+z_2^2}} \qquad (10)$$

Repeatability tests were also performed at the extreme temperatures of -275°F and +350°F. Due to limitation of using ball probes while inside the environmental chamber, measurements were taken after the joint was removed from the chamber. Glass wool was placed inside the hollow portion of the joint to minimize temperature loss when exposed to room temperature. Also, a ceramic wool blanket with cutouts for the nests and Torquer mechanism were added as soon as the joint was mounted to the table, as shown in Figure 28. This approach limited the temperature change (350 °F or -275 °F inside the environmental chamber) to a 30 °F change over the 5 minutes required to complete the two sets of 10 measurements. The results from the tests at extreme temperatures showed a precision an order of magnitude worse than measured at room temperature. The lower precision was likely due to joint surface temperature changes and the associated thermal expansion/contraction effects, as well as thermal distortions in the air surrounding the SMRs.

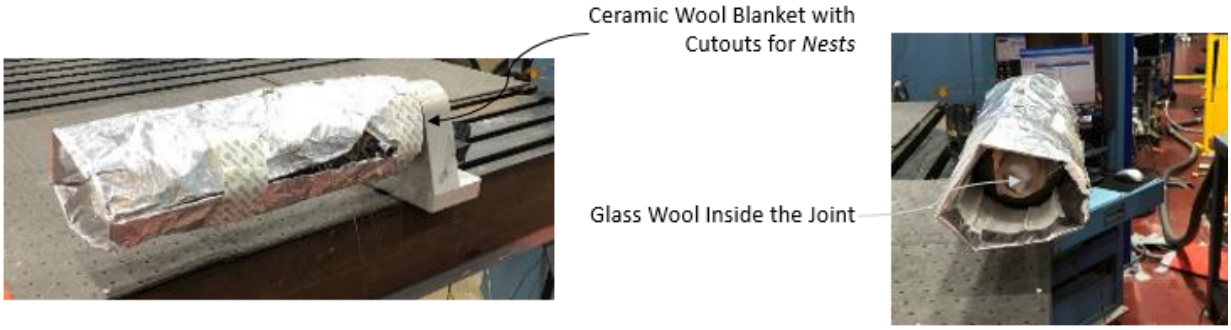

Figure 28. Test Setup for Repeatability Checks at Extreme Temperatures.

LESSONS LEARNED

The location of the LVDT support collars were crucial to the above tests in measuring displacements that were a small fraction of the manufacturer specified range. For axial tests, initially placing the LVDT collars on the load train led to inaccurate displacement measurements. Attachment of the collars directly to the body of the specimen resulted in valid load-displacement curves and correct stiffness measurements. For torsion tests, the surface distortions due to torsion loading of the joint specimen's non-symmetric cross section required judicious selection of the locations to which the collars were attached.

For the bending test, minimizing the bending below the test specimen would enable more bending for the test area. The current test fixture design includes a narrowing down at the test adaptor resulting in its lower moment of inertia than the test specimen. Therefore, changing the test fixture to have a cylindrical insert with a higher bending moment of inertia between the test specimen and the fixed base would improve the measurement of the joint's bending stiffness. A preliminary finite element analysis can also aid in the design.

For the initial joint assembly repeatability tests, a single laser tracker was used with the SMR being moved between two joint halves. The precision of this test setup was on the same order as the

rotation requirement between the joint halves. With two laser trackers and two SMRs, the test setup precision improved by a factor of 10 higher than the targeted requirement.

Since uniform contact between the joint halves affected their stiffness performance, it was essential to perform blue layout aid and inspection before commencing tests. Performing this activity earlier will capture the differences from manufacturing alone. Otherwise, wear at the interfaces may result from repeated assembly and disassembly during testing.

SUMMARY

Test systems were developed and customized to measure the mechanical behavior of the joints under tension, compression, bending, and torsion conditions for characterizing the performance of an ISA robotic joint across a range of on-orbit temperatures. In addition, a test system for measuring the repeatability of disassembling and re-assembling the joint specimens was developed. A key element associated with each of these test types was its ability to measure very small displacements over a wide range of temperatures.

The results from all these tests were useful for informing design changes for a structural joint system that requires high precision when deployed in space.

ACKNOWLEDGEMENTS

The authors would like to thank Steve Mark and Robert Wagner of AMA, Inc., for their expertise on finite element models and their technical advice on improving the test setups. We also thank Clarence Stanfield, Stewart Walker and Clayton Mills for test system assembly and test execution, and Dave Fahringer and Ellis Sherry were instrumental with machining the joints.

REFERENCES

[1]Roa, M., Nottensteiner, K., Wedler, A. and Grunwald, G., "Robotic Technologies for In-Space Assembly Operations", Advanced Space Technologies in Robotics and Automation Conference, Netherlands, 20-22 June 2017.

[2]Dorsey J. and Watson J., "Summary of LaRC 2-inch Erectable Joint Hardware Heritage Test Data", NASA-TM-2016-219189, March 2016.

[3]Lymer J. et. al., "Commercial Application of In-Space Assembly", AIAA Paper 2016-5236, September 2016.

[4]Belvin K., et. al., "In-Space Structural Assembly: Applications and Technology", AIAA Paper 2016-2163, January 2016.

[5]Calibration Task Description for Contract Displacement Transducers (DCDT, LVDT, Extensometers, Clip Gages), LMS-TD-8730.18, Revision A, Langley Research Center, Materials Research Lab, March 2016.

REPORT DOCUMENTATION PAGE

Form Approved
OMB No. 0704-0188

1. REPORT DATE *(DD-MM-YYYY)*	2. REPORT TYPE	3. DATES COVERED *(From - To)*
1-05-2019	Technical Memorandum	

4. TITLE AND SUBTITLE

In-Space Robotic Assembly Joint Characterization Approach

5a. CONTRACT NUMBER

5b. GRANT NUMBER

5c. PROGRAM ELEMENT NUMBER

6. AUTHOR(S)

Abraham, Nijo A.; Bird, Richard K.; Doggett, William R.; Roach, Timothy S.

5d. PROJECT NUMBER

5e. TASK NUMBER

5f. WORK UNIT NUMBER

216894.04.01.07.06

7. PERFORMING ORGANIZATION NAME(S) AND ADDRESS(ES)

NASA Langley Research Center
Hampton, VA 23681-2199

8. PERFORMING ORGANIZATION REPORT NUMBER

L-21024

9. SPONSORING/MONITORING AGENCY NAME(S) AND ADDRESS(ES)

National Aeronautics and Space Administration
Washington, DC 20546-0001

10. SPONSOR/MONITOR'S ACRONYM(S)

NASA

11. SPONSOR/MONITOR'S REPORT NUMBER(S)

NASA-TM-2019-220281

12. DISTRIBUTION/AVAILABILITY STATEMENT

Unclassified-
Subject Category 88
Availability: NASA STI Program (757) 864-9658

13. SUPPLEMENTARY NOTES

14. ABSTRACT

This paper describes the test systems and approaches developed to characterize the performance of a structural joint that is intended for robotic in-space assembly (ISA). The design of the joint is based on a heritage concept from National Aeronautics and Space Administration (NASA) Langley Research Center (LaRC) originally intended for structural assembly by astronauts during extravehicular activity (EVA). Its design was modified under a public-private partnership and is intended to accelerate the availability of, and reduce costs for the infusion of NASA developed technologies into commercial ISA systems. Test systems were developed to measure the axial, bending, and torsional stiffness of the joint at a wide range of temperatures. A test system was also developed to measure the reliability of the joint in terms of translation and rotation when disassembled and re-assembled in space. These test systems were used to characterize the joint behavior and provide performance data for the iterative joint design process. The paper also lists the lessons learned to aid testing of next generation robotic in-space assembly joints.

15. SUBJECT TERMS

Axial; Bending; In-Space Robotic Assembly; Joint Testing; Repeatability; Torsion

16. SECURITY CLASSIFICATION OF:			17. LIMITATION OF ABSTRACT	18. NUMBER OF PAGES	19a. NAME OF RESPONSIBLE PERSON
a. REPORT	b. ABSTRACT	c. THIS PAGE			STI Help Desk (email: help@sti.nasa.gov)
U	U	U	UU	31	19b. TELEPHONE NUMBER *(Include area code)* (757) 864-9658